Desalination and Water Treatment
www.deswater.com

doi: 10.1080/19443994.2014.990931

57 (2016) 2855–2869
February

Taylor & Francis
Taylor & Francis Group

Incipient crystallization of calcium carbonate on desalination membranes: dead-end filtration with agitation

S.T. Mitrouli[a,b], M. Kostoglou[a,b,*], A.J. Karabelas[a], A. Karanasiou[a]

[a]*Chemical Process and Energy Resources Institute, Centre for Research and Technology—Hellas, 6th km Charilaou-Thermi Road, GR 57001, Thermi-Thessaloniki, Greece, Tel. +30 2310 498184; Fax: +30 2310 498189; email: mitrouli@cperi.certh.gr (S.T. Mitrouli), Tel. +30 2310 997767; Fax: +30 2310 997759; email: kostoglu@chem.auth.gr (M. Kostoglou), Tel. +30 2310498181; Fax: +30 2310498189; email: karabaj@cperi.certh.gr (A.J. Karabelas), Tel. +30 2310498184; Fax: +30 2310498189; email: akaranasiou@cperi.certh.gr (A. Karanasiou)*

[b]*Division of Chemical Technology, School of Chemistry, Aristotle University of Thessaloniki, GR 54124 Thessaloniki, Greece*

Received 26 June 2014; Accepted 21 October 2014

ABSTRACT

The development of reliable criteria for determining the onset of scaling on desalination membranes is of high practical value. A novel approach to systematically investigate incipient membrane crystallization and scale-particle evolution was recently reported by this laboratory, involving modeling-relevant phenomena during membrane desalination and experiments, in well-controlled pressure cells operating in dead-end mode with no agitation. However, parallel studies have shown that flow conditions equivalent to those prevailing in real desalination membrane modules are obtained in pressure cells *with agitation*. Therefore, this work aims to employ the aforementioned approach to the more realistic case of membrane $CaCO_3$ scaling in dead-end desalination with agitation. Detailed data regarding incipient $CaCO_3$ scaling of desalination membranes were obtained, by analyzing scanning electron microscopy (SEM) images, for small bulk supersaturation ratios $S = 1$ to 4 and short filtration times (~30–90 min). Mean shear stresses at the membrane surface were similar to those prevailing in desalination modules. The data show that concentration polarization due to salt rejection strongly affects scale-particle growth rate, insignificantly influencing particle-number surface density. There is no evidence of a significant induction period in the nucleation and growth of scale-particles on the membrane surface. The initial $CaCO_3$ deposit flux, in mg/(m^2 min), exhibits a strong dependence on membrane surface supersaturation. Experimental data on the supersaturation-dependent scale evolution appear to significantly differ from predictions based on classical concepts of heterogeneous nucleation and growth, thus indicating that non-conventional nucleation is the dominant mechanism of the membrane-scale development.

Keywords: Incipient $CaCO_3$ scaling; Brackish water desalination; RO membranes; Particle size distribution; Supersaturation; Nucleation theory

*Corresponding author.

1. Introduction

Maximization of clean water recovery in membrane plants is pursued worldwide due to the diminishing water resources [1–3]. The percentage of clean water recovery in membrane desalination and water treatment processes essentially depends on the concentration and type of salts (dissolved in the feed water) and, in particular, on the sparingly soluble ones. The latter, beyond a certain limit of permeate recovery, tend to precipitate on the membrane due to supersaturation, with negative impact on plant performance. This problem of membrane "scaling" is particularly acute in the case of treating low salinity waters with dissolved scale-forming cations (including Ca, Mg, Sr, and Ba) as well as various anionic species (usually carbonate, sulfate, and phosphate) [1,4]. Calcium carbonate, which is dealt with in this study, is a commonly encountered membrane-scale compound.

In practice, the limits to permeate water recovery imposed by membrane scaling can be extended somewhat by the use of anti-scalants [5]; for instance, membrane manufacturers [6] recommend an upper limit on the Langelier saturation index (LSI) of a desalination plant concentrate (i.e. LSI < 1.8), which corresponds to a rather low supersaturation index SI for calcite (SI < ~2) *with the use of anti-scalants*. However, the latter are generally undesirable for economic and environmental reasons, and efforts are made to reduce their use. At present, a great deal of empiricism is involved in determining the degree of allowable permeate recovery (in essence, the degree of concentrate supersaturation in the membrane plant) usually in combination with the use of a certain dosage of anti-scalants. Progress in satisfactorily addressing this difficult problem, at the practical level, depends to a large extent on understanding the onset of scale formation on the membrane surface under conditions of water desalination.

Despite the very extensive literature on precipitation of sparingly soluble salts in the fluid bulk [7–10] and on various substrates [5,11–14], there are significant gaps (at both experimental and theoretical level) in our understanding of incipient crystalline scale formation on solid surfaces [15] and, in particular, *on semi-permeable membranes* during water desalination. From the experimental standpoint, at the allowable in desalination plants quite low bulk supersaturation ratio S of the aforementioned salts, there is uncertainty on whether an "induction period" of membrane scaling exists [16], as well as on how, and at which rate, the scale-particles initially develop (or deposit) and then grow on a "clean" desalination membrane. Most of the work on desalination membrane scaling has been carried out at relatively high supersaturations and/or for experimentation times beyond the initial phase of crystal generation, deposition, and growth on a virgin membrane surface [17–19]. These relatively long experimentation times in literature studies are essentially dictated by the scale detection and measurement techniques used. Moreover, the induction time is usually determined by measurements of either bulk fluid properties (i.e. fluid turbidity, conductivity, and Ca^{2+} concentration) or process parameters (e.g. flux decline) [17–20], which lack the required sensitivity [16] to observe the initially sparsely distributed micron-size scale particles on the membrane. At the theoretical level, our ability to predict true incipient scaling under realistic conditions is mainly hampered by two factors; i.e. (a) the multiple ionic species composition of natural feed waters, introducing uncertainty in equilibria calculations and (b) the complicated flow field within the spiral-wound membrane (SWM) modules of RO plants where spacers are inserted to separate the membranes and to create fluid passages. An approach to address the former problem [21] involves the use of an appropriate modeling framework in connection with available advanced equilibria computational codes. On the latter problem, significant progress has been made in recent years [22,23] in simulating the complicated flow field within the narrow passages of SWM modules. A detailed description has been obtained of the flow field and of mass transfer to the membrane surface within this complicated geometry as well as correlations for the pressure drop and mass transfer coefficient, which are essential for spatially detailed simulation of SWM performance at steady state [24] and for the more demanding spatiotemporal evolution of fouling [25] and scaling [26] in membrane modules.

The approach taken by the authors to investigate incipient membrane scaling involves detailed experimental work (employing scanning electron microscopy—SEM), at small fluid supersaturation and of relatively short duration, aiming at determining quantitatively the scale-particle development, as well as theoretical modeling to interpret the data by accounting for the temporal and spatial scale evolution. As a first step to implement this approach, the simple flow field of dead-end filtration *with no agitation* was employed [21] and experimental data on incipient $CaCO_3$ membrane scaling were obtained; furthermore, a modeling framework was developed, whereby the theoretically determined evolution of rejected species concentration at the membrane surface was coupled with a detailed kinetic model (also involving population balances) for predicting nucleation and particle growth on the membrane. Valuable insights were

obtained from this effort, indicating that incipient scaling at small bulk supersaturations is controlled by the fluid permeation. To proceed with the determination of nucleation/crystallization parameters, (for a particular physicochemical system) one needs detailed experimental data under well-controlled conditions. The dead-end high pressure filtration cell *with agitation* (very extensively used in membrane filtration research) is considered appropriate for this task; in fact, recent research [27] shows that it can provide a flow field with lateral convective currents which are equivalent to those prevailing in the real desalination (SWM) elements even though the flow structure is different in the two cases. Moreover, tests with the filtration cell under agitation are more convenient and less time-consuming than those in cross-flow desalination systems, for detailed experimental observations and determination of model parameters; such data are useful to validate and/or improve currently used theoretical models. However, it should be stressed that the more laborious cross-flow tests are still needed to obtain more realistic data on incipient membrane scaling [16] for comparison with the dead-end cell results. In view of the aforementioned state of the art, the scope of this work is to study experimentally incipient crystallization of calcium carbonate on desalination membranes, under well-controlled conditions of small initial supersaturations, in a dead-end cell with fluid agitation.

2. Equipment, materials and methods

Experiments to investigate incipient crystallization on desalination membranes were conducted, in dead-end filtration mode with agitation, using an experimental set-up, comprising three high-pressure stirred cells. For systematic data collection, these cells were operated simultaneously, under identical experimental conditions (with the exception of filtration time or stirring rate), as described in detail elsewhere [21,28]. The effective membrane area in each stirred cell was 9.1 cm^2. High-pressure nitrogen was used to control the applied pressure, in the range of 150–200 psi [~1,000 to ~1,380 kPa]. In the stirred test cell, containing the synthetic feed solution, milli-Q water was continuously supplied from a second pressure vessel to compensate for the permeate removal; thus, the chemical composition of the feed water inside the test cell remained essentially constant during the desalination test period, irrespective of the permeate withdrawal, which was generally small. The temperature was maintained constant in the tests. The majority of experiments was performed under a constant stirring rate of 250 rpm, while some tests were conducted under various stirring rates (60, 90 or 250 rpm) in order to assess the effect of flow shear stress on calcium carbonate crystal deposition on the membrane surface. The 250 rpm stirring rate was selected because it was recently shown [27] that it leads to a space-average shear stress at the membrane surface roughly equal to that prevailing in spacer-filled channels of SWM modules at usual cross-flow velocity ~15 cm/s. The permeate flux was determined by measuring the permeate mass through an electronic balance (PL602-S Mettler-Toledo AG, Switzerland), which was connected to a computer for data acquisition. A low-pressure reverse osmosis, thin film composite polyamide membrane (CPA2, Hydranautics, USA), was employed in this study. Membrane coupons in appropriate dimensions were cut from a commercial SWM element. After rinsing with distilled water, the coupons were stored in an aqueous solution of 0.75% $Na_2S_2O_5$ (sodium meta-bisulfite) and kept in a refrigerator.

The description for preparation of the synthetic solutions used in these tests and the experimental protocol can be found elsewhere [21]. The feed solution was well characterized, prior to filtration tests, by measuring pH, conductivity, and calcium concentration via a laboratory multi-parameter meter (inoLab 750 pH/ION/Cond multilab, WTW, Germany); turbidity was measured by a portable turbidimeter (HF Scientific Inc., DRT-15CE, USA). Additional measurements, including concentration of total dissolved solids (TDS) and total alkalinity, were performed on feed water [29]. The supersaturation ratio of feed solution was determined by a thermodynamic ion-association model (PHREEQC computer program, version 2.15.07) implementing the extension of the Debye–Hückel theory [30]. For these calculations, for low ionic strength solutions, the most complete literature database (*minteq.v4.dat)* available at present was employed [31], while for high ionic strength solutions the *pitzer.dat* database was used.

After the membrane preparation and compaction [21], the pressurized auxiliary vessel was filled with approx. 700 mL milli-Q water, whereas the pressure test cell was filled completely with approx. 300 mL synthetic feed water; the latter was fully characterized regarding physical properties and supersaturation ratio [21]. It should be pointed out that efforts were made to eliminate or minimize the free air volume above the aqueous solution (by totally filling the cell) in order to keep constant the solution pH during the filtration period [32].

The disk-type membrane coupons, after the termination of dead-end tests, were dried and prepared for SEM (SEM, JSM-6300 scanning electron microscope, JEOL Ltd., Japan) observations [21]. Additionally, in

some tests, the feed water and retentate solutions were filtered through a 0.2 μm mixed cellulose ester membrane. These filters were also prepared for SEM observations in order to determine the characteristics of calcium carbonate crystals existing (if any) in the bulk feed solution. Representative SEM images were retained for further processing. Qualitative chemical information about the precipitates on the membrane surface was obtained by the X-ray spectrometer unit (EDS, LINK ISIS, OXFORD) connected to the SEM system. For each test condition, usually 2–7 SEM pictures were processed with the "Image J" (v.1.43n, 2010) special software [33], a public domain Java image processing and analysis program, freely downloadable from Internet.

Table 1 summarizes the experimental conditions employed for investigating incipient $CaCO_3$ crystallization on the reverse osmosis membrane. The bulk supersaturation ratio S of the precipitate, regarding calcite, which was found to be the dominant crystalline phase, is defined as follows:

$$S = \left[\frac{(a_{Ca^{2+}})(a_{CO_3^{2-}})}{K_{SP}}\right]^{1/2} \quad (1)$$

where the quantities in parentheses are the activities of calcium and carbonate ions, respectively, computed by the PHREEQC code (version 2.15.07) [30]. The value of K_{SP} was also obtained through that software. The supersaturation index SI, alternatively employed in some publications, is defined as:

$$SI = 2 \cdot \log S \quad (2)$$

To determine the concentration of each ionic species (Ca^{2+}, HCO_3^-, Cl^-, Na^+) right at the membrane surface (c_w), and subsequently their activities through the PHREEQC software, the following equation is employed for each ion:

$$[c_w/c_b] = (1 - R) + R \cdot \exp(v_w/k_m) \quad (3)$$

where c_b, R and v_w are the known bulk species concentration, ion rejection (assuming $R = 1$ for complete salt rejection), and permeate flux, respectively. From measurements of mass transfer coefficients in the same type of stirred dead-end filtration cell [27], the following correlation was obtained:

$$Sh = 0.49 \cdot Re^{0.55} \cdot Sc^{0.33} \quad (4)$$

Here, Sh is the Sherwood number $\left(Sh = \frac{K_m \cdot D_H}{D}\right)$, where k_m is the average mass transfer coefficient (m/s), D_H is the hydraulic diameter, which for the case of stirred dead-end cell is equal to the radius r of active membrane surface, D is the diffusion coefficient of each ion, Sc is the Schmidt number, defined as $Sc = \frac{v}{D}$, and v is the kinematic viscosity of the liquid. The Reynolds number is given as $Re = \frac{\omega \cdot r^2}{v}$, where ω is the angular velocity (rad/s).

The values of bulk supersaturation ratio of calcium carbonate, selected for these tests, were very near the saturation limits, i.e. in the narrow range $S = 1$–4, in order to investigate incipient crystallization phenomena right at the membrane surface. It is considered that *the bulk supersaturation remained effectively constant* throughout the tests since the pH variation during these tests was always less than 0.2 and the species consumption for solids formation was negligible, estimated by an overall mass balance. To examine nucleation and particle growth by SEM, each set of tests comprised of experiments with identical initial conditions and different durations, thus allowing measurement of crystallization parameters (mainly crystal sizes and number surface densities) at three different times; in most cases, a set of three such tests per experiment are reported here (Table 1). Table 1 also summarizes tests performed from 30 up to 120 min but under various stirring rates to assess the effect of flow shear stresses and mass transfer coefficient on calcium carbonate crystallization on the membrane surface. Finally, the permeate flux imposed in the tests, which was essentially the driving force for membrane surface crystallization, was within the range ~24–40 L/(m^2 h).

3. Experimental results

A summary of experimental results is provided in Table 2, including calcium carbonate crystal parameters, particle surface density, and initial deposit mass flux (estimated by SEM image processing) as well as pH and turbidity values measured for bulk solution and retentate. Turbidity values for the bulk (retentate) exhibit a significant gradual increase for the usual test period extending from feed solution preparation up to 180 min thereafter. It should be pointed out that tests with increased retentate turbidity are not taken into account in the following data analysis. Turbidity is likely due to homogeneous nucleation of calcium carbonate in the bulk, although one cannot exclude some contribution of small particles detached from the membrane surface. From the measured number concentration of feed bulk-particles in some tests (73D and 78D, Table 2), it is concluded that this concentration is relatively small and (if all such particles were deposited) would make insignificant *direct*

contribution to the total scale-particle mass measured on the membrane. Indeed, a fair estimate of the deposition rate of bulk $CaCO_3$ particles on the membrane surface can be obtained using the approach described elsewhere [16]. For a typical range of deposition coefficients $k_D = 10^{-5}$ to 10^{-3} cm/s (rather conservative for order of magnitude calculations) and using the average value 0.10 mg/L for particle mass concentration in the feed-fluid (data for tests no. 73D and 78D in Table 2), one obtains bulk particle deposition fluxes on the membrane 0.6×10^{-3} to 0.6×10^{-1} mg/(m^2 min), respectively. It is concluded that these deposition fluxes, for the observed particle sizes in the range 1–3 μm, are one to three orders of magnitude smaller than the measured mean initial mass fluxes [0.4–5.1 mg/(m^2 min), Table 2].

Estimates of bulk supersaturation ratio (S_b) and of supersaturation ratio right at the membrane surface (S_w) are also listed in Table 2. The supersaturation ratios (with respect to calcite) right at the membrane surface, S_w, are 7 to 56% greater than the corresponding values determined for the bulk solution, depending on experimental conditions; the smaller shear stresses lead to greater increase in surface supersaturation ratio, compared to bulk supersaturation ratio, as expected.

In Fig. 1, two typical crystal size distributions of particles detected on the desalination (CPA2) membrane surfaces are presented, from tests performed under similar experimental condition (initial bulk supersaturation ratio, $S \sim 3.0$, stirring rate, permeate flux and ionic strength) but different filtration times (30 and 60 min). From such distributions, the mean (d_{50}) as well as the d_5 and d_{95} crystal sizes (listed in Table 2) were determined. As one would expect, for a longer filtration period, the distribution is shifted toward larger crystal sizes. Considering the short filtration period of these tests (30–60 min), these data confirm that the incipient membrane-scaling process evolves with time with practically no induction period.

Fig. 2 depicts crystal size distributions from tests conducted under almost identical experimental conditions (regarding initial bulk supersaturation ratio S_b, permeate flux, stirring rate), with the exception of the ionic strength of the feed solution. Samples from the desalination membrane obtained from the test with the higher ionic strength exhibit a very narrow crystal size distribution characterized by smaller particle diameters compared to deposited calcium carbonate particles corresponding to smaller ionic strength solution. Moreover, particles of different morphology, as depicted in SEM images in Fig. 3, were observed in the test with the feed solution of the higher ionic strength. Indeed, for a 60 min filtration period, particles of irregular shape were observed on the membrane from tests with the high ionic strength solution compared to rhombohedral calcite crystals corresponding to solution with the lower ionic strength, even though the supersaturation ratio was somewhat smaller in the latter case. It should also be pointed out that the ratio of calcium activity to carbonate ions

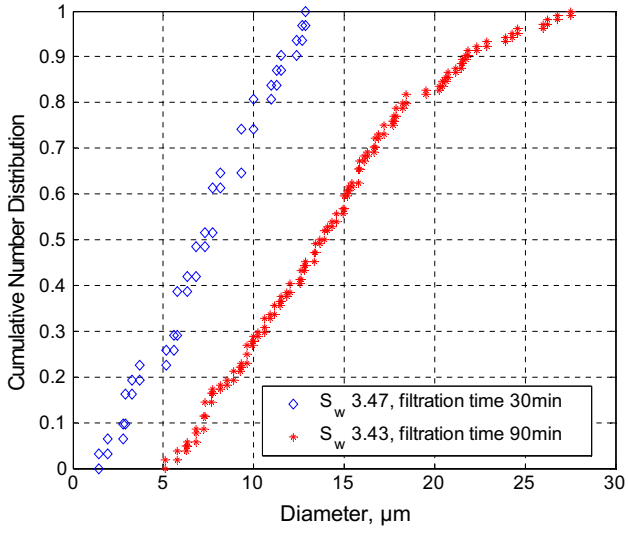

Fig. 1. Crystal size distributions from tests of different filtration duration; $S_w \sim 3.45$, test duration 30 (test no. 54D) and 90 min (test no. 55D).

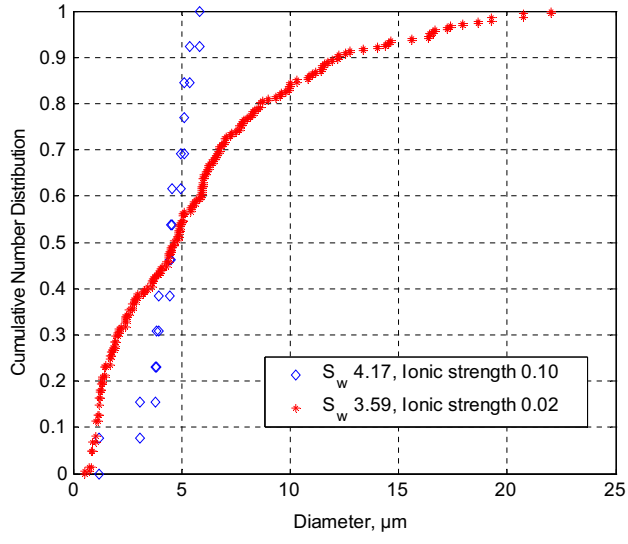

Fig. 2. Crystal size distributions from tests of different ionic strengths; $S_w \sim 3.6$ and 4.2, test duration 60 min. Test nos. 73D and 78D.

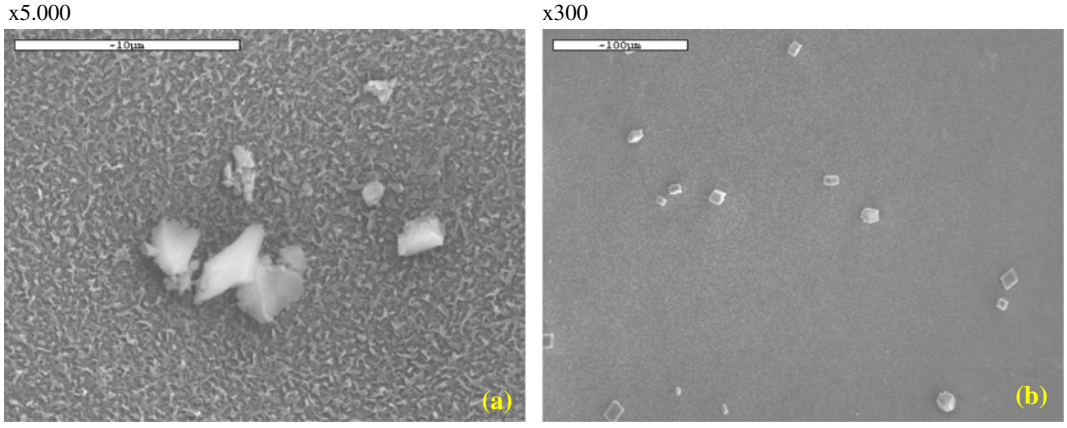

Fig. 3. SEM images from desalination membrane surface after filtration of (a) high ionic strength (test no. 73D) and (b) low ionic strength solution (test no. 78D).

activity for the high ionic strength solution is seven times greater than that calculated for the low ionic strength solution. Consequently, it is assumed that this difference in crystal habit is due to the different background electrolyte solution (NaCl) concentration that may interfere with the process of crystal growth on the membrane surface; it is also noted that similar observations are reported [34–36] on the effect of calcium to carbonate activity ratio on crystal growth.

The measured particle number distributions (Table 2) are converted to a mean initial $CaCO_3$ mass flux (in mg/(m^2 min)), computed over the test period, which is a parameter of theoretical and practical significance. These data are plotted in Fig. 4 vs. wall supersaturation ratio, S_w. It is interesting that, despite the scatter, these data display a rather strong dependence of calcium carbonate mass flux on surface supersaturation, S_w. A similar trend was also observed in $CaCO_3$ scaling experiments recently performed in continuous cross-flow filtration mode [16], in a narrow spacer-filled channel simulating conditions prevailing in SWM modules.

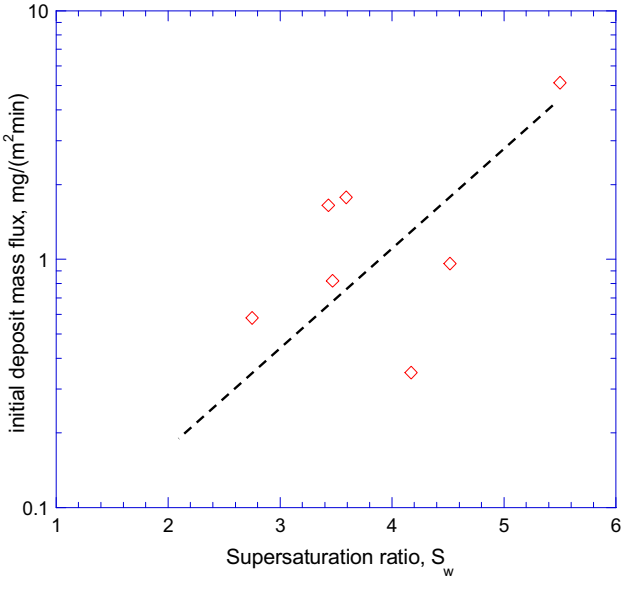

Fig. 4. Initial deposit mass flux [mg $CaCO_3$/(m^2 min)] vs. wall supersaturation ratio; in most tests, stirring rate 250 rpm.

Fig. 5(a) depicts data for the size distribution of particles detected in the feed solution sample, which was collected 30 min after the solution preparation; these data characterize the size of particles developing during this period. In the same figure, data are presented for the size distribution of particles observed in a retentate solution sample, which was collected from the stirred cell when the scaling experiment was terminated (data from test no. 78D with S_w 3.61). In this particular test, particle size distributions for feed solution and retentate are very similar (apart from some larger crystals detected in the feed water sample), implying that bulk particle growth occurs at a very small rate during the filtration period. Fig. 5(b) includes data for size distribution of particles observed on the membrane surface after the same filtration test (78D). It is important to note that particles on the membrane surface are quite larger than particles observed in the retentate solution for the same time period. This is evidence that the conditions at the membrane surface are more favorable for crystal growth than those in the bulk. These particles are either formed (as nuclei) right on the membrane surface, and subsequently grow, or originate from small particles existing in the bulk that deposit on the membrane surface, becoming surface particles, also

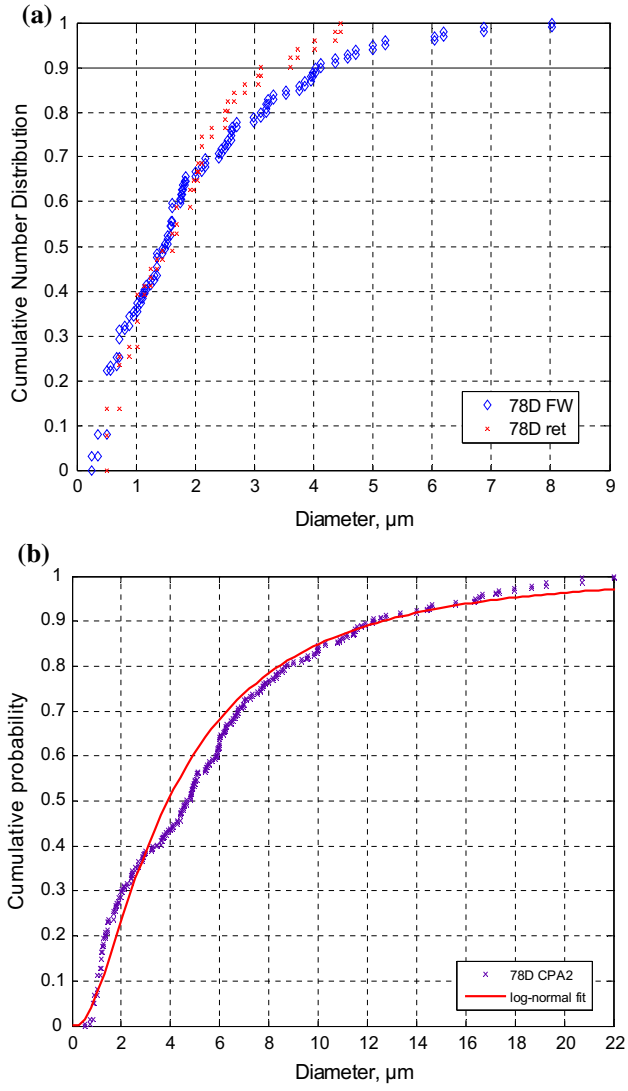

Fig. 5. (a) Particle size distributions from samples of feed solution (30 min after preparation) and retentate (after test termination, t = 60 min), (b) Particle size distribution from desalination membrane surface (t = 60 min). Test no. 78D.

growing with time. It should be also noted that there is satisfactory fitting of the distributions in Fig. 5 with a typical log-normal-type expression.

There is evidence that (as expected) the effect of stirring rate significantly affects the incipient crystallization process, through its direct effect on the concentration boundary layer. Such evidence is presented in Fig. 6, which depicts the size distributions of particles detected on the membrane surfaces for two tests after 60 min filtration time. Specifically, by comparing test nos. 70D and 71D (Tables 1 and 2), which were performed under exactly the same experimental conditions except for stirring rate (250 and 60 rpm,

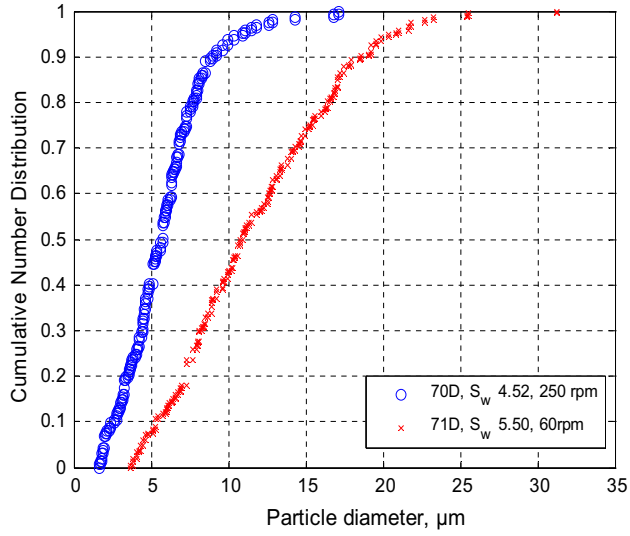

Fig. 6. Particle size distributions from tests with different stirring rates; i.e. 250 (test no. 70D) and 60 rpm (test no. 71D), respectively. Filtration time 60 min for both tests.

respectively), calcium carbonate particles almost twice as large are observed on the membrane surface from the test with the smaller stirring rate; however, there is a rather insignificant difference in particle-number surface density. Consequently, higher initial deposit mass flux (5.13 mg/(m^2 min)) was calculated for the test with smaller stirring rate.

Regarding the effect of supersaturation ratio on scale-particle size, upon inspection of the data in Table 2 (e.g. tests 54D and 57D), it is observed that there is no gradual increase in scale-particle size with the supersaturation ratio, under the conditions tested near saturation. Moreover, the surface particle number density seems to be insensitive to supersaturation ratio variations (mainly for the lower ratios S tested). At this point, one should note that there is significant scatter in the data due to experimental error, mainly associated with the selection of membrane sample-image size for statistical treatment. Indeed, to obtain a representative number of particles (especially at the smallest ratio S), a small image magnification is required which results in relatively low image resolution, thus introducing errors in particle size determination. Consequently, the best approach would be to obtain SEM images with the same magnification, for all tests performed; however, this is constrained by the particle size distribution on the membrane surface.

It is known that there are at least six different phases of calcium carbonate: three anhydrous crystalline polymorphs (the most thermodynamically stable calcite with the least Gibbs free energy, the metastable aragonite and the unstable vaterite, which may also be

Table 1
Experimental conditions of dead-end filtration with agitation; supersaturation ratio S_b and index SI correspond to bulk conditions

Test ID	Filtration time (min)	ΔP (psi)	Stirring rate (rpm)	Flux (L/m^2 h)	v_w (μm/s)	[Ca^{2+}] (mg/L)	[HCO_3^-] (mg/L)	[CO_3^{2-}]$_{total}$ (mg/L)	Ionic strength (M)	Supersat. ratio, S_b	Supersat. index, SI
51D	30	200	250	40.0	11.1	1,005	384	774.0	0.10	1.02	0.02
52D	90	200	250	38.5	10.7	1,005	384	774.0	0.10	1.02	0.02
53D	180	200	250	39.0	10.8	990	345	694.2	0.10	0.95	−0.04
54D	30	150	250	26.7	7.4	991	656	777.6	0.10	2.95	0.94
55D	90	150	250	26.5	7.4	991	656	777.6	0.10	2.95	0.94
56D	180	150	250	28.0	7.8	1,050	659	787.2	0.10	2.95	0.94
57D	30	150	250	30.0	8.3	1,060	479	671.4	0.10	1.82	0.52
58D	90	150	250	30.5	8.5	1,060	479	671.4	0.10	1.82	0.52
59D	180	150	250	24.4	6.8	1,020	549	774.6	0.10	1.88	0.55
65D	30	150	90	27.0	7.5	923	418	813.6	0.10	1.06	0.05
66D	30	150	60	25.0	6.9	923	390	786.0	0.10	0.99	−0.01
70D	60	150	250	38.0	10.6	239	210	204.2	0.02	3.67	1.13
71D	60	150	60	33.5	9.3	239	210	204.2	0.02	3.67	1.13
72D	120	150	60	37.0	10.3	239	210	204.2	0.02	3.67	1.13
73D	60	150	250	26.0	7.2	907	647	733.2	0.10	3.09	0.98
76D	60	170	250	29.0	8.1	978	534	643.8	0.11	2.34	0.74
78D	60	165	250	23.5	6.5	249	204	200.1	0.02	3.39	1.06

formed under kinetic control reactions) [37] and three hydrated forms (crystalline monohydrate (monohydrocalcite), crystalline hexahydrate (ikaite, $CaCO_3{\cdot}6H_2O$)) and an amorphous calcium carbonate hydrate [38]. Several SEM pictures of calcium carbonate polymorphs that have grown on the membrane, under various test conditions, are presented in Fig. 7. The membrane surface supersaturation ratio S_w, the duration of each test and the stirring rate are also marked therein. It should be noted that in these figures, two magnifications were used for each test on purpose; i.e. the higher magnification was necessary to examine the morphology of a few crystals, whereas the smaller one allowed the statistical analysis regarding crystal size distribution.

Upon inspection of the SEM images and other data obtained from these experiments, the following additional observations can be made:

(1) One observes crystals of calcite, such as typical rhombohedral (also incomplete and staircase-like crystals in some cases as shown in Fig. 7(h) and (n)) and spherical or hexagonal-plate vaterite crystals (observed at high supersaturation ratio after 180 min since feed solution preparation) and their agglomerates. For tests conducted under low supersaturarion ratio ($S = 1.29$), very few crystals of irregular shape were observed (Fig. 7(b)) after 30 min of filtration. It is assumed that these irregular crystals are representative of a metastable stage, whereby the initial amorphous $CaCO_3$ particles, while growing, tend to be transformed to the stable regular crystals observed at later times [7]. These irregular crystals appear to have a shorter height compared to their width, i.e. the contact angles between these particles and the membrane surface is low, providing an indication that they almost completely adhere to the surface; this shape indicates that heterogeneous nucleation and growth processes right on the membrane surface dominate at incipient scaling (see also Ref. [15]).

(2) For tests with *slightly supersaturated feed solutions* ($S_w = 1.22$–1.29, test nos. 51D–53D performed under 250 rpm stirring rate, and $S_w = 1.36$–1.40, test nos. 65D–66D performed at the lower stirring rates), very few crystals of calcium carbonate were detected only in the periphery of the circular membrane sector examined under SEM. This fact may be related to the relatively small shear stresses in that membrane region [27], which are likely associated with increased local concentration polarization and supersaturation ratio, thus, leading to a non-uniform scale deposition pattern. It may be also added that under these

Table 2
Summary of experimental results; the surface supersaturation ratio S_w is determined on the basis of feed pH

Test ID	Filtration time (min)	SEM images	Particles per image	d_5/d_{95} (μm)	d_{50} (μm)	Particle surf. density (#/m^2)	Solution pH		Solution turbidity		Bulk supersat. ratio, S_b	Surface supersat. ratio, S_w	Mass flux mg/(m^{2}min)
							Feed	Retentate	Feed	Retentate			
51D	30	2	~25	2.8/16.2	6.2	3.5E+07	6.19	6.34	0.10	0.12	1.02	1.29	–
52D	90	1	~21	5.2/12.6	6.8	2.0E+07	6.19	6.36	0.10	0.40	1.02	1.27	–
53D	180	2	~15	2.4/15.9	7.0	1.8E+07	6.19	6.52	0.12	0.55	0.95	1.22	–
54D	30	3	~10	2.4/12.5	7.3	2.1E+07	6.89	6.92	0.14	0.18	2.95	3.47	0.82
55D	90	4	~26	6.4/24.2	13.8	2.5E+07	6.89	6.97	0.14	0.37	2.95	3.43	1.65
56D	180	4	~698	10.3/29.5	15.2	7.1E+08	6.87	7.09	0.10	0.70	2.95	3.55	–
57D	30	4	~32	4.4/19.4	9.6	3.1E+07	6.58	6.69	0.11	0.14	1.82	2.16	–
58D	90	2	Very few crystals	ND*	ND	ND	6.58	6.75	0.11	0.35	1.82	2.16	–
59D	180	4	~68	3.6/18.9	6.3	6.6E+07	6.57	6.76	0.12	0.60	1.88	2.21	–
65D	30			ND/ND	ND	ND	6.22	6.35	0.55	0.88	1.06	1.40	–
66D	30	3	Very few crystals	ND/ND	ND	ND	6.19	6.30	0.40	0.58	0.99	1.36	–
70D	60	7	~23	2.0/10.5	5.7	5.1E+07	8.04	7.90	0.22	0.30	3.67	4.52	0.96
71D	60	7	~30	4.5/20.6	10.9	6.4E+07	8.04	8.02	0.22	0.22	3.67	5.50	5.13
72D	120	7	~363	3.9/18.3	7.4	2.2E+09	8.04	7.90	0.22	2.50	3.67	5.75	–
73D	60	4	~4	1.5/5.8	4.5	1.1E+08	7.04	7.17	–	–	3.09	4.17	0.35
0.2 μm_Conc.	60	5	~31	1.5/5.6	2.3	0.18 (mg/L)**	–	–	–	–	–	–	
76D	60	6	~12	1.2/7.1	2.2	8.0E+08	6.90	7.00	0.10	0.22	2.34	2.75	0.58
0.2 μm_Conc.	60	–	–	ND	ND	ND	–	–	–	–	–	–	
78D	60	22	~11	0.9/16.5	4.7	1.5E+08	7.96	7.83	0.09	0.10	3.39	3.59	1.78
0.2 μm_F.W.	30	6	~17	0.4/5.1	1.5	0.03 (mg/L)**	–	–	–	–	–	–	
0.2 μm_Conc	60	6	~9	0.5/4.0	1.6	0.02 (mg/L)**	–	–	–	–	–	–	

*ND: Not Determined; **Particle concentration in fluid/concentrate, mg/L.

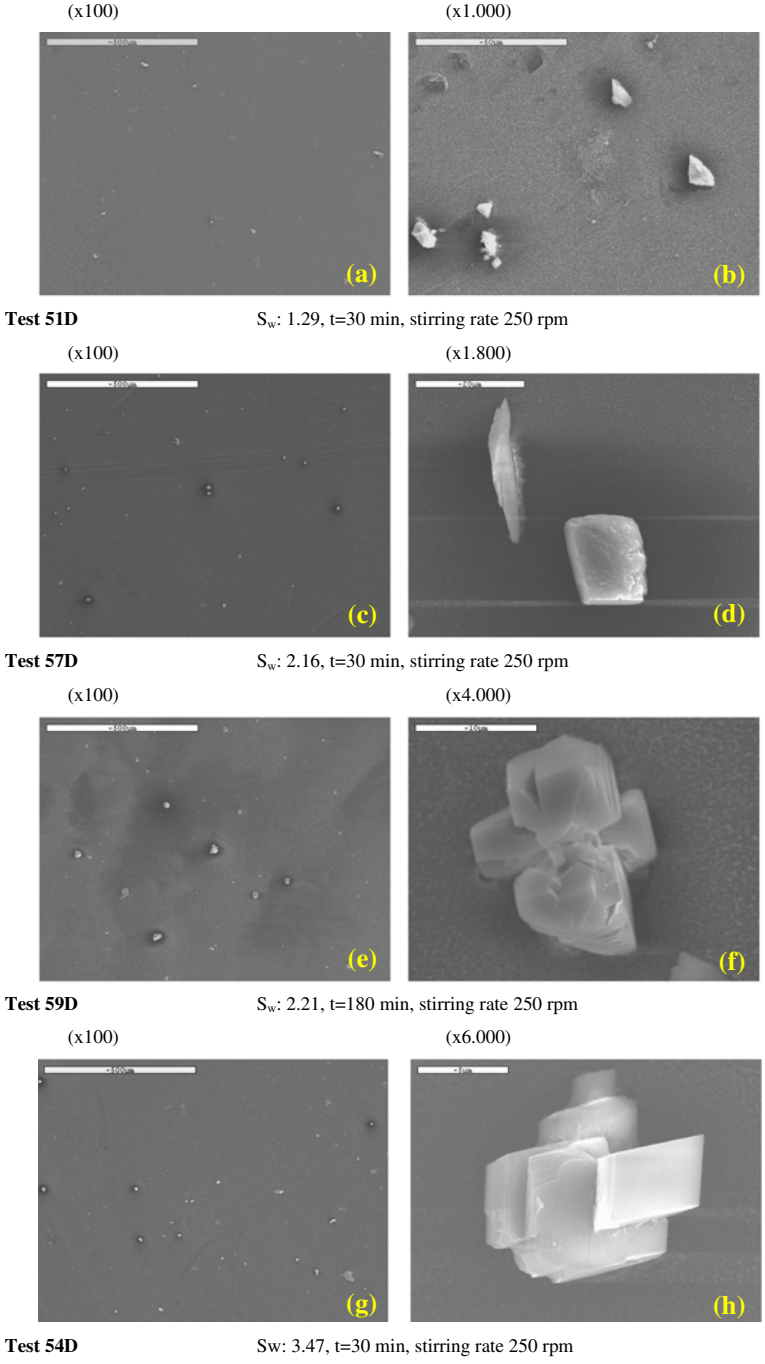

Fig. 7. Incipient calcite growth on a RO membrane for various supersaturation ratios.

conditions, there is no evidence of significant induction period for nucleation.

(3) For tests conducted with *solutions at higher supersaturation* (test nos. 54D–59D, $S_w = 2.16$–2.21 and 3.43–3.57, respectively), crystals of calcium carbonate on the membrane were detected in membrane samples from the first 30 min of filtration. These crystals were larger and of more complicated shape. For the longer duration tests (90 and 180 min, test nos. 55D, 56D, 58D and 59D, respectively) depicted in Fig. 7, the crystals are larger in size and in much greater numbers, as one would have expected. Finally, crystals

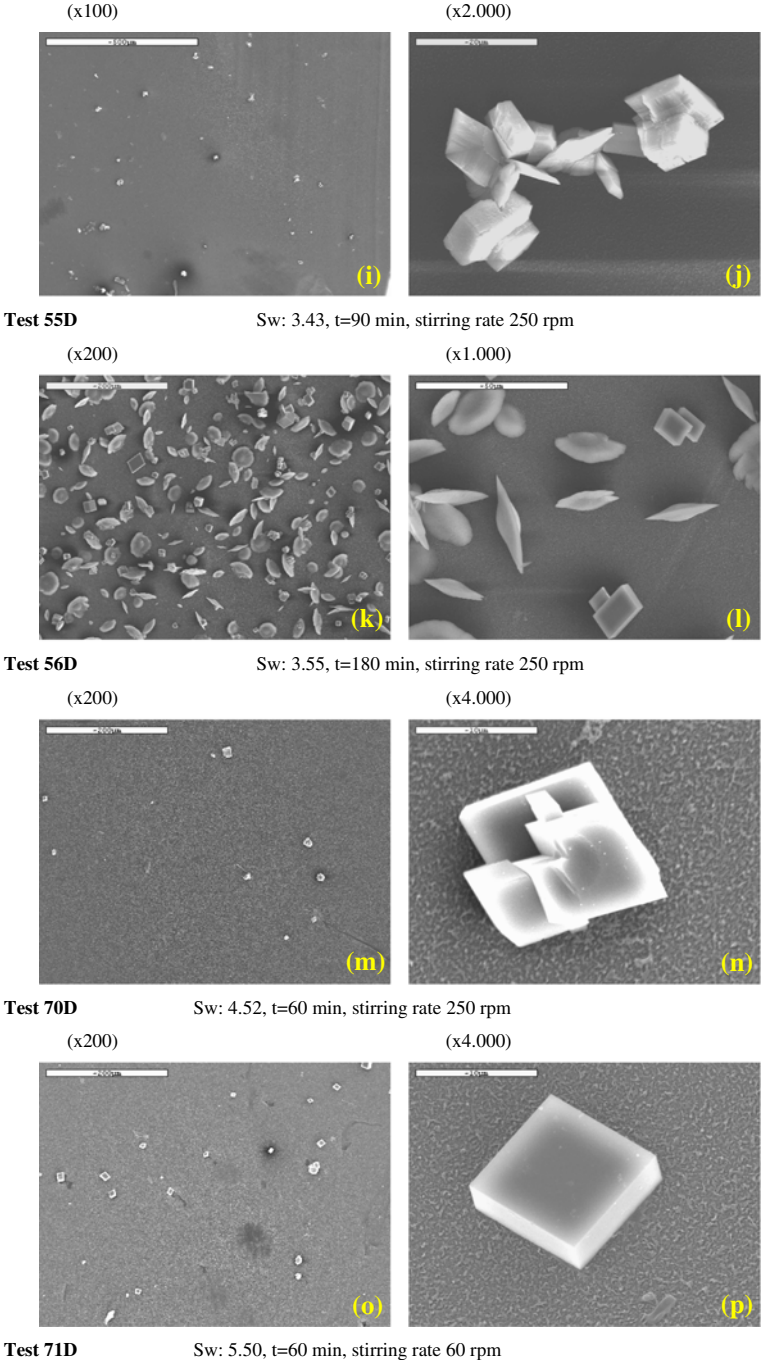

Fig. 7. (*Continued*).

observed on the membrane surface from test no. 73D, where feed solution of higher ionic strength and calcium and bicarbonate concentrations were employed, compared to feed solution of test no. 78D, were smaller and with a very narrow size distribution (see also Fig. 2).

4. Discussion of the results

Measurements of bulk particle numbers revealed that their concentration was too small to have a significant direct contribution to the surface mass evolution. Additionally, by employing experimental data obtained at the end of the tests and performing a

global mass balance, it was found that in all cases the experiments were actually carried out under constant active species concentration in time and the scale-development process did not influence the concentration polarization. This implies that the situation in stirred cell desalination is quite different compared to that of no agitation (i.e. lack of lateral convection) where the wall supersaturation tends to increase to rather high values, with subsequent reduction due to ionic species consumed by fast precipitation [21]. However, the stirred cell precipitation conditions are similar to those prevailing in desalination SWM modules where the precipitation rate is relatively small and has no influence on the species concentration profile [16]. In the stirred cell, the mass transfer coefficient is generally a weak function of the radial coordinate [27]; however, for the relatively small levels of concentration polarization, of the present experiments, radially-averaged quantities can be employed.

According to the classical nucleation theory, the surface nucleation rate J (units: $\#/m^2/s$) is a function of the local supersaturation of the form $J = A\ \exp(-B/\ln^2(S_w))$, where A and B are dimensionless parameters dependent on the scale and substrate material [39]. The volumetric particle growth rate G (units: m^3/s) is a function of the local supersaturation and of the particle volume x; i.e. $G = k_g(S_w)x_\alpha$ where k_g has units $m^{3-3\alpha}/s$. The exponent α is 1/3 for diffusion-dominated growth and 2/3 for reaction-dominated growth [39]. Denoting N as the surface particles number density ($\#/m^2$) and M as the scale volume per unit surface (m^3/m^2), the following equations can be derived for their evolution:

$$\frac{dN}{dt} = J \tag{5}$$

$$\frac{dM}{dt} = Jx_c + Nk_g\left(\frac{M}{N}\right)^{\alpha} \tag{6}$$

where t is the time and x_c is the nucleus size. Typically, the nucleus diameter is much less than a micrometer [39]; thus, taking into account the particle diameters measured in the present work, the first term of the right-hand side of Eq. (6) can be safely ignored. The solution of the simplified system for an initially clean membrane leads to:

$$N = Jt \tag{7}$$

$$M = k_g^{1/(1-\alpha)}J\left(\frac{1-\alpha}{2-\alpha}\right)^{1/(1-\alpha)}t^{(2-\alpha)/(1-\alpha)} \tag{8}$$

The average particle diameter d is proportional to $(M/N)^{1/3}$ and thus to $t^{1/(3-3\alpha)}$. The slow growth rates of the present experiments suggest that the dominant growth mode is the reaction so $\alpha = 2/3$ (exponent for surface reaction growth rate) and $d \propto t$. The foregoing mathematical analysis of the model dependencies reveals that, for constant bulk species concentration and insignificant bulk particle deposition, the surface particle number and their average diameter should increase approx. linearly with time. However, the experimentally determined evolution of these parameters with time, for the same or similar conditions, does not appear to be in agreement with theory, exhibiting a weaker dependence in most cases. Another discrepancy appears to arise regarding the dependence of the nucleation rate on supersaturation ratio. Indeed, Table 2 shows that the surface particle number density for the case of bulk supersaturation 2.95 (test 54/55D) appears to be similar to that for supersaturation 1.02 (test 51/52D), whereas the theory predicts a strong supersaturation dependence. It should be noted that a similar discrepancy between theory and experiment has been also observed [16] in the case of $CaCO_3$ precipitation in cross-flow test sections simulating SWM module operation. The situation is different in the absence of stirring where the developing high values of supersaturation at the membrane surface lead to better agreement between theory and experiments [21].

Possible reasons of the discrepancy between theory and experiments in the system studied are outlined here. The nucleation theory has been tested in the past by employing *integral* quantities (and using always adjustable constants). It should be noted, however, that the development of advanced experimental techniques permits the acquisition of detailed data (in the temporal and spatial sense); attempts to simultaneously fit such data reveal the shortcomings of the classical theory, as recently noted by Chen et al. [40]. Furthermore, it will be recalled that the precipitation theory has been developed for large supersaturation conditions; indeed, the condition of large supersaturation is included in the definition of precipitation [39]. Therefore, the existing theory may be inappropriate for describing incipient precipitation under the conditions of small supersaturation associated with the corresponding small nucleation rates of the present experiments. It will be added that questions about the validity of the classical nucleation theory for precipitation of calcium carbonate have been recently raised in the literature [41,42].

Another aspect in the development of conventional models of membrane scaling (outlined above) needs attention; specifically, a basic premise in the

development of such models is that the entire membrane surface is uniform and has the same affinity for nucleation. However, it seems that this may not be the case. Indeed, there may be a distribution of affinities (or a distribution of local surface energies) that can explain the nonlinear time dependence of the measured particle number. Such a distribution of nucleation-site affinity has theoretical support in the literature [43]. There is also experimental evidence regarding the membrane surface spatial non-uniformity (obtained in this laboratory [28]), which is manifested in the non-uniform permeate flux and salt rejection. Therefore, it appears that there is scope for pursuing the development of a new particle nucleation model capable of describing successfully the temporal evolution of surface particles on desalination membranes.

5. Concluding remarks

Experiments were performed in the dead-end filtration mode with agitation, which is a relatively convenient way to obtain experimental data under conditions equivalent to those prevailing in cross-flow membrane modules. Detailed data regarding incipient calcium carbonate scaling of reverse osmosis desalination membranes were obtained, using analysis of SEM images, in a narrow range of bulk supersaturation ratio $S = 1$ to ~4 and short times (~30–90 min) since solution preparation. The main results of these experiments are summarized as follows:

(1) Data from size distributions of particles dispersed in feed and retentate solutions as well as of scale-particles on the desalination membrane surface provide evidence that calcium carbonate scale-particles are either formed (as nuclei) right on the membrane surface (and subsequently grow) or originate from small particles existing, at low concentrations, in the bulk that deposit on the membrane surface, becoming surface particles, also growing with time.

(2) The increasing surface particle sizes, measured at different times (i.e. 30 and 60 min) since membrane contact with the slightly supersaturated solution, provide evidence that an evolving scale-particle growth process takes place with practically no induction period.

(3) Particles of calcium carbonate observed on the membrane surfaces were of various forms such as typical calcite rhombohedral (also incomplete and staircase-like crystals in some cases) as well as spherical or hexagonal-plate vaterite crystals (observed at the higher supersaturation ratio) and their agglomerates. The latter are indicative of the early stages of crystallization before the stable form of calcite totally dominates.

(4) The initial $CaCO_3$ deposit mass flux, in $mg/(m^2 min)$, computed over the short test period, which is a parameter of theoretical and practical significance, exhibits a rather strong dependence on membrane surface supersaturation S_w.

(5) The imposed shear stress through stirring significantly affects the scale-particle growth, as expected. Much larger calcium carbonate particles (and mass deposition rates) were observed on the membrane surface in tests with reduced stirring rate, all other experimental conditions being the same; however, such influence on the particle-number surface density appeared to be insignificant.

(6) The results of analysis of supersaturation ratio effects on scale-particle size and their number density on the membrane surface, based on the classical heterogeneous nucleation/growth theory, is at variance with the experimental results, indicating that possibly a non-classical type of nucleation mechanism prevails in membrane-scale formation.

References

[1] J. Thompson, A. Rahardianto, H. Gu, M. Uchymiak, A. Bartman, M. Hedrick, D. Lara, J. Cooper, J. Faria, P.D. Christofides, Y. Cohen, Rapid field assessment of RO desalination of brackish agricultural drainage water, Water Res. 47 (8) (2013) 2649–2660.

[2] N. Misdan, W.J. Lau, A.F. Ismail, Seawater reverse osmosis (SWRO) desalination by thin-film composite membrane—Current development, challenges and future prospects, Desalination 287 (2012) 228–237.

[3] C. Charcosset, A review of membrane processes and renewable energies for desalination, Desalination 245 (2009) 214–231.

[4] G. Greenberg, D. Hasson, R. Semiat, Limits of RO recovery imposed by calcium phosphate precipitation, Desalination 183 (2005) 273–288.

[5] D. Hasson, R. Semiat, Scale control in saline and wastewater desalination, Isr. J. Chem. 46(1) (2006) 97–104.

[6] Nitto Denko—Hydranautics, Technical Application Bulletin (TAB) 111, Chemical Pretreatment for RO and NF, 2008.

[7] J.W. Mullin, Crystallization, third ed., Butterworth-Heinemann, Oxford, 1993.

[8] O. Sohnel, J. Garside, Precipitation: Basic Principles and Industrial Applications, Butterworth-Heinemann, Oxford, 1992.
[9] A.E. Nielsen, Kinetics of Precipitation, Pergamon Press, London, 1964.
[10] N. Spanos, P.G. Koutsoukos, Kinetics of precipitation of calcium carbonate in alkaline pH at constant supersaturation. Spontaneous and seeded growth, J. Phys. Chem. B 102(34) (1998) 6679–6684.
[11] E. Dalas, J. Kallitsis, P.G. Koutsoukos, The crystallization of calcium carbonate on polymeric substrates, J. Cryst. Growth 89(2–3) (1988) 287–294.
[12] E. Dalas, P. Klepetsanis, P.G. Koutsoukos, The overgrowth of calcium carbonate on poly(vinyl chloride-co-vinyl acetate-co-maleic acid), Langmuir 15(23) (1999) 8322–8327.
[13] E. Dalas, P.G. Klepetsanis, P.G. Koutsoukos, Calcium carbonate deposition on cellulose, J. Colloid Interface Sci. 224(1) (2000) 56–62.
[14] M.G. Lioliou, C.A. Paraskeva, P.G. Koutsoukos, A.C. Payatakes, Heterogeneous nucleation and growth of calcium carbonate on calcite and quartz, J. Colloid Interface Sci. 308 (2007) 421–428.
[15] H. Wang, V. Alfredsson, J. Tropsch, R. Ettl, T. Nylander, Formation of $CaCO_3$ deposits on hard surfaces—Effect of bulk solution conditions and surface properties, ACS Appl. Mater. Interfaces 5 (2013) 4035–4045.
[16] S. Mitrouli, A.J. Karabelas, A. Karanasiou, M. Kostoglou, Incipient calcium carbonate scaling of desalination membranes in narrow channels with spacers —Experimental insights, J. Membr. Sci. 425–426 (2013) 48–57.
[17] S. Lee, J. Kim, C.-H. Lee, Analysis of $CaSO_4$ scale formation mechanism in various nanofiltration modules, J. Membr. Sci. 163(1) (1999) 63–74.
[18] D. Hasson, A. Drak, R. Semiat, Inception of $CaSO_4$ scaling on RO membranes at various water recovery levels, Desalination 139(1–3) (2001) 73–81.
[19] D. Hasson, H. Shemer, I. Brook, I. Zaslavschi, R. Semiat, Scaling propensity of seawater in RO boron removal processes, J. Membr. Sci. 384 (2011) 198–204.
[20] N. Pomerantz, Y. Ladizhansky, E. Korin, M. Waisman, N. Daltrophe, J. Gilron, Prevention of scaling of reverse osmosis membranes by "Zeroing" the elapsed nucleation time. Part I. Calcium sulfate, Ind. Eng. Chem. Res. 45 (2006) 2008–2016.
[21] A.J. Karabelas, M. Kostoglou, S.T. Mitrouli, Incipient crystallization of sparingly soluble salts on membrane surfaces: The case of dead-end filtration with no agitation, Desalination 273(1) (2011) 105–117.
[22] C.P. Koutsou, S.G. Yiantsios, A.J. Karabelas, Direct numerical simulation of flow in spacer-filled channels: Effect of spacer geometrical characteristics, J. Membr. Sci. 291 (1–2) (2007) 53–69.
[23] C.P. Koutsou, S.G. Yiantsios, A.J. Karabelas, A numerical and experimental study of mass transfer in spacer-filled channels: Effects of spacer geometrical characteristics and Schmidt number, J. Membr. Sci. 326 (2009) 234–251.
[24] M. Kostoglou, A.J. Karabelas, Comprehensive simulation of flat-sheet membrane element performance in steady state desalination, Desalination 316 (2013) 91–102.
[25] M. Kostoglou, A.J. Karabelas, A mathematical study of the evolution of fouling and operating parameters throughout membrane sheets comprising spiral wound modules, Chem. Eng. J. 187 (2012) 222–231.
[26] M. Kostoglou, A.J. Karabelas, Modeling scale formation in flat-sheet membrane modules during water desalination, AIChE J. 59(8) (2013) 2917–2927.
[27] C.P. Koutsou, A.J. Karabelas, Shear stresses and mass transfer at the base of a stirred filtration cell and corresponding conditions in narrow channels with spacers, J. Membr. Sci. 399–400 (2012) 60–72.
[28] S.T. Mitrouli, A.J. Karabelas, N.P. Isaias, Polyamide active layers of low pressure RO membranes: Data on spatial performance non-uniformity and degradation by hypochlorite solutions, Desalination 260 (2010) 91–100.
[29] APHA, Standard methods for the examination of water and wastewater, seventeenth ed., Port City Press, Baltimore, MD, 1989, 2540C, pp. 2-74–2-75, 2320B, pp. 2-35–2-39.
[30] D.L. Parkhurst, C.A.J. Appelo, User's Guide to phreeqc (version 2)—A Computer Program for Speciation, Batch-reaction, One-dimensional Transport, and Inverse Geochemical Calculations, U.S. Department of the Interior, U.S. Geological Survey, 1999.
[31] T. Todorov, D. Rabadjieva, S. Tepavitcharova, New thermodynamic database for more precise simulation of metal species in natural waters, J. Univ. Chem. Technol. Metall. 41(1) (2006) 97–102.
[32] R. Beck, M. Seiersten, J.-P. Andreassen, The constant composition method for crystallization of calcium carbonate at constant supersaturation, J. Cryst. Growth 380 (2013) 187–196.
[33] T.A. Ferreira, W. Rasband, The ImageJ users guide, version 1.43, 2010.
[34] E. Ruiz-Agudo, C.V. Putnis, L. Wang, A. Putnis, Specific effects of background electrolytes on the kinetics of step propagation during calcite {1014} growth, Geochim. Cosmochim. Acta 75 (2011) 3803–3814.
[35] K. Larsen, K. Bechgaard, S.L.S. Stipp, The effect of the Ca^{2+} to CO_3^{2-} activity ratio on spiral growth at the calcite $\{10\bar{1}4\}$ surface, Geochim. Cosmochim. Acta 74 (2010) 2099–2109.
[36] J. Paquette, R.J. Reeder, Relationship between surface-structure, growth-mechanism, and trace-element incorporation in calcite, Geochim. Cosmochim. Acta 59 (1995) 735–749.
[37] D. Zhao, Y. Zhu, F. Li, Q. Ruan, S. Zhang, L. Zhang, F. Xu, Polymorph selection and nanocrystallite rearrangement of calcium carbonate in carboxymethyl chitosan aqueous solution: Thermodynamic and kinetic analysis, Mater. Res. Bull. 45 (2010) 80–87.
[38] P. López-Arce, L.S. Gómez-Villalba, S. Martínez-Ramírez, M. Álvarez de Buergo, R. Fort, Influence of relative humidity on the carbonation of calcium hydroxide nanoparticles and the formation of calcium carbonate polymorphs, Powder Technol. 205 (1–3) (2011) 263–269.
[39] J.A. Dirksen, T.A. Ring, Fundamentals of crystallization: Kinetic effects on particle size distributions and morphology, Chem. Eng. Sci. 46 (1991) 2389–2427.
[40] K. Chen, L. Goh, G. He, P.J.A. Kenis, C.F. Zukoski III, R.D. Braatz, Identification of nucleation rates in

droplet-based microfluidic systems, Chem. Eng. Sci. 77 (2012) 235–241.
[41] Q. Hu, M.H. Nielsen, C.L. Freeman, L.M. Hamm, J. Tao, J.R.I. Lee, T.Y.J. Han, U. Becker, J.H. Harding, P.M. Dove, J.J. De Yoreo, The thermodynamics of calcite nucleation at organic interfaces: Classical vs. non-classical pathways, Faraday Discuss. 159 (2012) 509–523.
[42] D. Gebauer, M. Kellermeier, J.D. Gale, L. Bergström, H. Cölfen, Pre-nucleation clusters as solute precursors in crystallisation, Chem. Soc. Rev. 43 (2014) 2348–2371.
[43] E. Curcio, V. Curcio, G. Profio, E. Fontananova, E. Drioli, Energetics of protein nucleation on rough polymeric surfaces, J. Phys. Chem. B 114 (2010) 13650–13655.